Electronic Supplementary Material (ESI) for Catalysis Science & Technology.
This journal is © The Royal Society of Chemistry 2019

Electronic Supplementary Information

Efficient asymmetric synthesis of chiral alcohols using high 2-propanol-tolerant alcohol dehydrogenase *Sm*ADH2 via an environmental friendly TBCR system

Zeyu Yang, Hengwei Fu, Wenjie Ye, Youyu Xie, Qinghai Liu, Hualei Wang* and Dongzhi Wei*

[a]State Key Laboratory of Bioreactor Engineering, New World Institute of Biotechnology, East China University of Science and Technology, Shanghai 200237, PR China

*Corresponding author:

Hua-Lei Wang: hlwang@ecust.edu.cn

**Corresponding author:

Dong-Zhi Wei: dzhwei@ecust.edu.cn

Table S1. Specific primes of ADHs library for PCR.

Entry	Enzyme	Accession number	Function	Sequence	
1	*Sm*ADH1	WP_088024587.1	Zinc-binding alcohol dehydrogenase	forward	5′-GGAATTC**CATATG**AAAGCCGTCGCCCTG-3′
				reverse	5′-CGC**GGATCC**CTAATCGTCCCAGCCCGC-3′
2	*Sm*ADH2	WP_088028380.1	SDR family oxidoreductase	forward	5′-GGAATTC**CATATG**ATTGATTACCAGTTGACCGG-3′
				reverse	5′-CGC**GGATCC**TCACTGCGCCAGGTAGCC-3′
3	*Sm*ADH3	SNW06321.1	L-threonine 3-dehydrogenase	forward	5′-GGAATTC**CATATG**GCGCAGCAAACGATG-3′
				reverse	5′-CGC**GGATCC**TCAATTCCAGCTCAACACCACC-3′
4	*Sm*ADH4	WP_065199584.1	3-oxoacyl-ACP reductase	forward	5′-GGAATTC**CATATGA**GCAAGCCCCTGCAG-3′
				reverse	5′-CGC**GGATCC**TTACGGCATGTACATGCCGC-3′
5	*Sm*ADH5	WP_088025739.1	3-hydroxybutyrate dehydrogenase	forward	5′-GGAATTC**CATATG**TTCAGTGGAAAGGTTGCG-3′
				reverse	5′-CGC**GGATCC**CTAGCGTGCGGTCCAGCC-3′
6	*Sm*ADH6	WP_088025845.1	3-oxoacyl-ACP reductase	forward	5′-GGAATTC**CATATG**TTCGGCGGCCAGCC-3′
				reverse	5′-CGC**GGATCC**TCAGTCCCGCACCAGTCC-3′
7	*Sm*ADH7	WP_088025997.1	Glutathione-dependent dehydrogenase	forward	5′-GGAATTC**CATATG**GGTCGCTCCTGCAGC-3′
				reverse	5′-CGC**GGATCC**TCAAGGTGTCAATACGATCTTGC-3′
8	*Sm*ADH8	WP_088026041.1	Glucose 1-dehydrogenase	forward	5′-CGC**GGATCC**ATGTCGTTCCAGGACAAGGTG-3′
				reverse	5′-CCC**AAGCTT**TCAGGAGAAGTAGGTGCCGC-3′
9	*Sm*ADH9	WP_088028365.1	SDR family oxidoreductase	forward	5′-GGAATTC**CATATG**ACCCTCTCCCCCACC-3′
				reverse	5′-CGC**GGATCC**TTACACCATCCCGCCATTG-3′
10	*Sm*ADH10	WP_088026620.1	SDR family oxidoreductase	forward	5′-GGAATTCCATATGCGCCTGAACAACAAGATC-3′
				reverse	5′-CGCGGATCCTCAGGTACGGGTGATCGACAC-3′
11	*Sm*ADH11	WP_088026393.1	SDR family oxidoreductase	forward	5′-GGAATTC**CATATG**AGTTTCAAGGCACTGCTGA-3′
				reverse	5′-CCG**GAATTC**TCAGGCATTCACATCCACGA-3′
12	*Sm*ADH12	WP_088026622.1	NADP-dependent oxidoreductase	forward	5′-GGAATTC**CATATG**TCCGATCCCTCGACCA-3′
				reverse	5′-CCG**GAATTC**TCAATCCAGCTTCACCACCAG-3′
13	*Sm*ADH13	WP_088026797.1	Acryloyl-CoA reductase	forward	5′-GGAATTC**CATATG**GCCCCCACCACCCC-3′
				reverse	5′-CCG**GAATT**CTCAGTCGATCCGCACCACG-3′
14	*Sm*ADH14	WP_088026836.1	SDR family oxidoreductase	forward	5′-GGAATTC**CATATG**GATCTGGATCTTGAAGGGC-3′
				reverse	5′-CGC**GGATCC**CTAGTGCGCGAAGTAGTGCATG-3′
15	*Sm*ADH15	WP_088027062.1	Acetoacetyl-CoA reductase	forward	5′-GGAATTC**CATATG**ACCCTTCGTATTGCATACG-3′
				reverse	5′-CGC**GGATCC**TTACCCCATGTACAGGCCACC-3′
16	*Sm*ADH16	WP_088027088.1	S-(hydroxymethyl)glutathione dehydrogenase	forward	5′-GGAATTC**CATATG**AAGTCCCGTGCCGCC-3′
				reverse	5′-CGC**GGATCC**TCAGTAGTGGACCACCGAACG-3′
17	*Sm*ADH17	WP_032129891.1	NAD(P)-dependent alcohol dehydrogenase	forward	5′-GGAATTC**CATATG**TCCCTCGCCCGTGGT-3′
				reverse	5′-CGC**GGATCC**TCAGGCGGCGTTCTTCATC-3′
18	*Sm*ADH18	WP_088027240.1	NAD(P)-dependent alcohol dehydrogenase	forward	5′-GGAATTC**CATATG**AACGACAACAACGCAACG-3′
				reverse	5′-CGC**GGATCC**TTACGCCGCGATGCGC-3′
19	*Sm*ADH19	WP_088027403.1	SDR family oxidoreductase	forward	5′-GGAATTC**CATATG**ACCCAGCAACGGTGG-3′
				reverse	5′-CGC**GGATCC**TCAGAACCCGTAGCGCAGG-3′
20	*Sm*ADH20	WP_088028365.1	SDR family oxidoreductase	forward	5′-GGAATTC**CATATG**ACCCTCTCCCCCACC-3′
				reverse	5′-CGC**GGATCC**TCAGAGCATGCCTCCGTTG-3′
21	*Sm*ADH21	WP_088028150.1	Zinc-binding alcohol dehydrogenase	forward	5′-GGAATTC**CATATG**CGCGCCATTGCCTAC-3′
				reverse	5′-CGC**GGATCC**TTACCAGCCTTCCAGCACG-3′
22	*Sm*ADH22	WP_088028265.1	SDR family oxidoreductase	forward	5′-GGAATTC**CATATG**CAGCCAATTTCTCGTATTTC-3′
				reverse	5′-CGC**GGATCC**TCAGCAGCGCGCGTCCAC-3′
23	*Sm*ADH23	WP_088025540.1	SDR family oxidoreductase	forward	5′-GGAATTC**CATATG**AGTGCCTGGCCATCGA-3′
				reverse	5′-CGC**GGATCC**TCACTCGCCGGGAAACGC-3′
24	*Sm*ADH24	WP_049400332.1	SDR family oxidoreductase	forward	5′-GGAATTC**CATATG**AATGGGATGCTGACGC-3′
				reverse	5′-CGC**GGATCC**TCAAGCGACGCCTGCGGT-3′
25	*Sm*ADH25	WP_014036829.1	SDR family oxidoreductase	forward	5′-GGAATTC**CATATG**AACACCCATCAGAACAAGATC-3′
				reverse	5′-CGC**GGATCC**TCACCATGGCAGCACCTCG-3′
26	*Sm*ADH26	WP_088025758.1	SDR family oxidoreductase	forward	5′-GGAATTC**CATATG**AAATTGATGGTCATCGGC-3′
				reverse	5′-CGC**GGATCC**TCAGTAGCGCGGGTCGGC-3′
27	*Sm*ADH27	ARQ89731.1	3-oxoacyl-ACP reductase	forward	5′-GGAATTC**CATATG**GCAACGGATCCGGCC-3′
				reverse	5′-CCG**GAATTC**TCAGCCCATCAACACCTGG-3′
28	*Sm*ADH28	WP_110712157.1	SDR family oxidoreductase	forward	5′-GGAATTC**CATATG**CAGCTGTCTTCCGTACGT-3′
				reverse	5′-CGC**GGATCC**TCACTTCGGAGCGAGGCG-3′
29	*Sm*ADH29	WP_088026079.1	FMN-dependent LLM class oxidoreductase	forward	5′-GGAATTC**CATATG**ACCATCGGCTACCACG-3′
				reverse	5′-CGC**GGATCC**CTATACGTGGCTGGCTGCC-3′
30	*Sm*ADH30	WP_088026081.1	Glucose 1-dehydrogenase	forward	5′-GGAATTC**CATATG**GCCCTGCCCGACTAC-3′
				reverse	5′-CGC**GGATCC**CTACAGCGTCGCAGCGCC-3′

Table S2. Screening novel *Sm*ADHs.

Entry	Enzyme	Coenzyme dependence	Relative activity (%)		*ee* (%)
			IPA	EAA	
1	*Sm*ADH1	NADH	nd.	13	nd.
2	*Sm*ADH2	NADH	100.0	100	99.9 (*R*)
3	*Sm*ADH3	-	nd.	nd.	nd.
4	*Sm*ADH4	NADPH	nd.	62	50.8(*S*)
5	*Sm*ADH5	NADPH	7.1	19	98.6 (*R*)
6	*Sm*ADH6	NADH	nd.	51	99.9 (*R*)
7	*Sm*ADH7	NADH	nd.	74	93.4(*R*)
8	*Sm*ADH8	NADH	nd.	69	31.3(*S*)
9	*Sm*ADH9	NADPH	1.2	55	99.3 (*R*)
10	*Sm*ADH10	-	nd.	nd.	nd.
11	*Sm*ADH11	NADPH	nd.	15	47.2 (*S*)
12	*Sm*ADH12	-	nd.	nd.	nd.
13	*Sm*ADH13	NADPH	3.6	66	82.9(*R*)
14	*Sm*ADH14	NADH	nd.	11	nd.
15	*Sm*ADH15	NADPH	nd.	36	99.9 (*S*)
16	*Sm*ADH16	NADH	nd.	46	85.1 (*R*)
17	*Sm*ADH17	-	nd.	nd.	nd.
18	*Sm*ADH18	NADH	nd.	31	24.7(*R*)
19	*Sm*ADH19	NADPH	nd.	40	73.8(*S*)
20	*Sm*ADH20	NADPH	nd.	14	99.9 (*R*)
21	*Sm*ADH21	NADH	nd.	62	99.6 (*R*)
22	*Sm*ADH22	-	nd.	nd.	nd.
23	*Sm*ADH23	-	nd.	nd.	nd.
24	*Sm*ADH24	NADPH	11.1	28	99.9 (*R*)
25	*Sm*ADH25	NADPH	nd.	72	92.9 (*R*)
26	*Sm*ADH26	-	nd.	nd.	nd.
27	*Sm*ADH27	-	nd.	nd.	nd.
28	*Sm*ADH28	NADH	nd.	35	99.6(*R*)
29	*Sm*ADH29	NADPH	nd.	22	99.9 (*S*)
30	*Sm*ADH30	-	nd.	nd.	nd.

[a] Relative activites measured using crude *Sm*ADHs under the standard assay protocol and expressed as percentages referred to *Sm*ADH2.
[b] Not detected.

Table S3. Effects of metal ions and EDTA on *Sm*ADH2.

	Concentration (mM)	*R*elative activity[a] (%)
Blank		100
EDTA	2	97
LiCl	2	94
KCl	2	82
$MgCl_2$	2	51
$CaCl_2$	2	50
$ZnCl_2$	2	36
$MnCl_2$	2	95
$FeCl_2$	2	77
$FeCl_3$	2	59
$CuCl_2$	2	24
$NiCl_2$	2	63
$CoCl_2$	2	22
$BaCl_2$	2	47

[a] Relative activites measured using purified *Sm*ADH2 and expressed as percentages referred to the Blank. Reaction conditions: purified *Sm*ADH2 was cultivated in PBS (100 mM, pH 7.0) containing different reagents (Li^+, K^+, Mg^{2+}, Ca^{2+}, Zn^{2+}, Mn^{2+}, Fe^{2+}, Fe^{3+}, Cu^{2+}, Ni^{2+}, Co^{2+} and Ba^{2+}) and EDTA (final concentration 2 mM) for 60 min at 30 °C. The enzyme activities were evaluated under standard conditions, using EAA as a model substrate.

Table S4. Asymmetric reduction of EAA with lyophilised *E.* coli Cells of *Sm*ADH2[a].

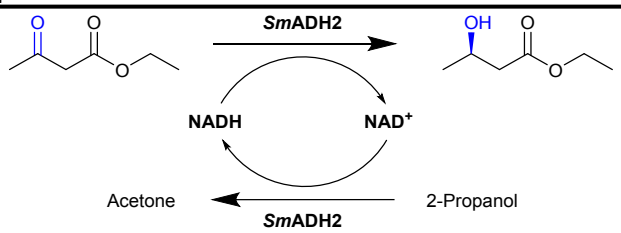

Entry	Reactor[b]	Ketone		NAD+	Cell	Time	Conv.[c]	*ee*[c]	Yield
		(g L^{-1})	(M)	(mM)	(g L^{-1})	(h)	(%)	(%)	(%)
1	TSTR	650	5	0.5	50	24	95	*R*(99.9)	93
2	TBCR	650	5	0.5	50	1.5	100	*R*(99.9)	93
3	TBCR	780	6	0.5	50	2	100	*R*(99.9)	93
4	TBCR	780	6	0.2	30	2	100	*R*(99.9)	93
5	TBCR	780	6	0	20	2.5	100	*R*(99.9)	93

[a] Reaction conditions: 10 ml PBS (100 mM, pH 7.0), 200–500 mg lyophilized cells, 0–5 µmol NAD+, 6.5–7.8 g EAA and 4.8–5.7 ml 2-propanol (1.25 equiv.) were placed in TSTR and TBCR separately and reacted at 30 °C for 24 h.
[b] Bioreductions performed in a conical flask reactor (TSTR) system (Entry 1) and a thermostatic bubble column reactor (TBCR) system (Entry 2–5).
[c] Conversion and *ee* values determined by GC analysis (Table S5)

Table S5. HPLC and GC analytic conditions and corresponding chromatographic columns for chiral alcohol products and acetone.

Product	Chiral column	Conditions
(*R*,*S*)-P1	CP-Chirasil-Dex CB (25 m×0.32 mm, 0.25 µm, Agilent, USA)	70 °C; Inc./dec. 250 °C; flow rate: 0.7 ml min^{-1}; nitrogen
(*R*,*S*)-P2	CP-Chirasil-Dex CB (25 m×0.32 mm, 0.25 µm, Agilent, USA)	70 °C; Inc./dec. 250 °C; flow rate: 0.7 ml min^{-1}; nitrogen
(*R*,*S*)-P3	CP-Chirasil-Dex CB (25 m×0.32 mm, 0.25 µm, Agilent, USA)	160 °C; Inc./dec. 250 °C; flow rate: 0.8 ml min^{-1}; nitrogen
(*R*,*S*)-P4	CP-Chirasil-Dex CB (25 m×0.32 mm, 0.25 µm, Agilent, USA)	80 °C; Inc./dec. 250 °C; flow rate: 0.6 ml min^{-1}; nitrogen
(*R*,*S*)-P5	CP-Chirasil-Dex CB (25 m×0.32 mm, 0.25 µm, Agilent, USA)	80 °C; Inc./dec. 250 °C; flow rate: 0.6 ml min^{-1}; nitrogen
(*R*,*S*)-P6	CP-Chirasil-Dex CB (25 m×0.32 mm, 0.25 µm, Agilent, USA)	85 °C; Inc./dec. 250 °C; flow rate: 0.7 ml min^{-1}; nitrogen
(*R*,*S*)-P7	CP-Chirasil-Dex CB (25 m×0.32 mm, 0.25 µm, Agilent, USA)	90 °C 2 min, 5 °C min^{-1}, 160 °C; Inc./dec. 250 °C ; 1.0 ml min^{-1}; nitrogen
(*R*,*S*)-P8	CP-Chirasil-Dex CB (25 m×0.32 mm, 0.25 µm, Agilent, USA)	90 °C 2 min, 5 °C min^{-1}, 160 °C; Inc./dec. 250 °C ; 1.0 ml min^{-1}; nitrogen
(*R*,*S*)-P9	CP-Chirasil-Dex CB (25 m×0.32 mm, 0.25 µm, Agilent, USA)	90 °C; Inc./dec. 250 °C; flow rate: 0.7 ml min^{-1}; nitrogen
(*R*,*S*)-P10	CP-Chirasil-Dex CB (25 m×0.32 mm, 0.26 µm, Agilent, USA)	100 °C; Inc./dec. 250 °C; flow rate: 0.7 ml min^{-1}; nitrogen
(*R*,*S*)-P11	Chiralcel OD-H column (0.46 mm×250 mm, 5 µm, Diacel, Japan)	hexane/2-propanol (95:5, v/v); flow rate: 1 mL min^{-1}; 210 nm
(*R*,*S*)-P12	Chiralcel OB-H column (0.46 mm×250 mm, 5 µm, Diacel, Japan)	hexane/2-propanol (95:5, v/v); flow rate: 1 mL min^{-1}; 210 nm
(*R*,*S*)-P13	Chiralcel OD-H column (0.46 mm×250 mm, 5 µm, Diacel, Japan)	hexane/2-propanol (95:5, v/v); flow rate: 1 mL min^{-1}; 210 nm
(*R*,*S*)-P14	Beta DEX™ 120 (30 m×0.25 mm, 0.25 µm, Supelco, USA)	120 °C; Inc./dec. 280 °C; flow rate: 0.8 ml min^{-1}; nitrogen
(*R*,*S*)-P15	Beta DEX™ 120 (30 m×0.25 mm, 0.25 µm, Supelco, USA)	150 °C; Inc./dec. 280 °C; flow rate: 0.8 ml min^{-1}; nitrogen
(*R*,*S*)-P17	Beta DEX™ 120 (30 m×0.25 mm, 0.25 µm, Supelco, USA)	170 °C; Inc./dec. 280 °C; flow rate: 0.8 ml min^{-1}; nitrogen
(*R*,*S*)-P20	Beta DEX™ 120 (30 m×0.25 mm, 0.25 µm, Supelco, USA)	120 °C; Inc./dec. 280 °C; flow rate: 0.7 ml min^{-1}; nitrogen
(*R*,*S*)-P21	Beta DEX™ 120 (30 m×0.25 mm, 0.25 µm, Supelco, USA)	150 °C; Inc./dec. 280 °C; flow rate: 0.7 ml min^{-1}; nitrogen
(*R*,*S*)-P22	Chiralcel OD-H column (0.46 mm×250 mm, 5 µm, Diacel, Japan)	hexane/2-propanol (95:5, v/v); flow rate: 0.8 mL min^{-1}; 254 nm
(*R*,*S*)-P23	Chiralcel OB-H column (0.46 mm×250 mm, 5 µm, Diacel, Japan)	hexane/2-propanol (98:2, v/v); flow rate: 1 mL min^{-1}; 210 nm
(*R*,*S*)-P24	CP-Chirasil-Dex CB (25 m×0.32 mm, 0.25 µm, Agilent, USA)	110 °C; Inc./dec. 250 °C; flow rate: 0.6 ml min^{-1}; nitrogen
(*R*,*S*)-P25	CP-Chirasil-Dex CB (25 m×0.32 mm, 0.26 µm, Agilent, USA)	140 °C; Inc./dec. 250 °C; flow rate: 0.6 ml min^{-1}; nitrogen
(*R*,*S*)-P26	Chiralcel OB-H column (0.46 mm×250 mm, 5 µm, Diacel, Japan)	hexane/2-propanol (95:5, v/v); flow rate: 1.0 mL min^{-1}; 254 nm
(R,S)-P27	Beta DEX™ 120 (30 m×0.25 mm, 0.25 µm, Supelco, USA)	130 °C; Inc./dec. 280 °C; flow rate: 0.8 ml min-1; nitrogen

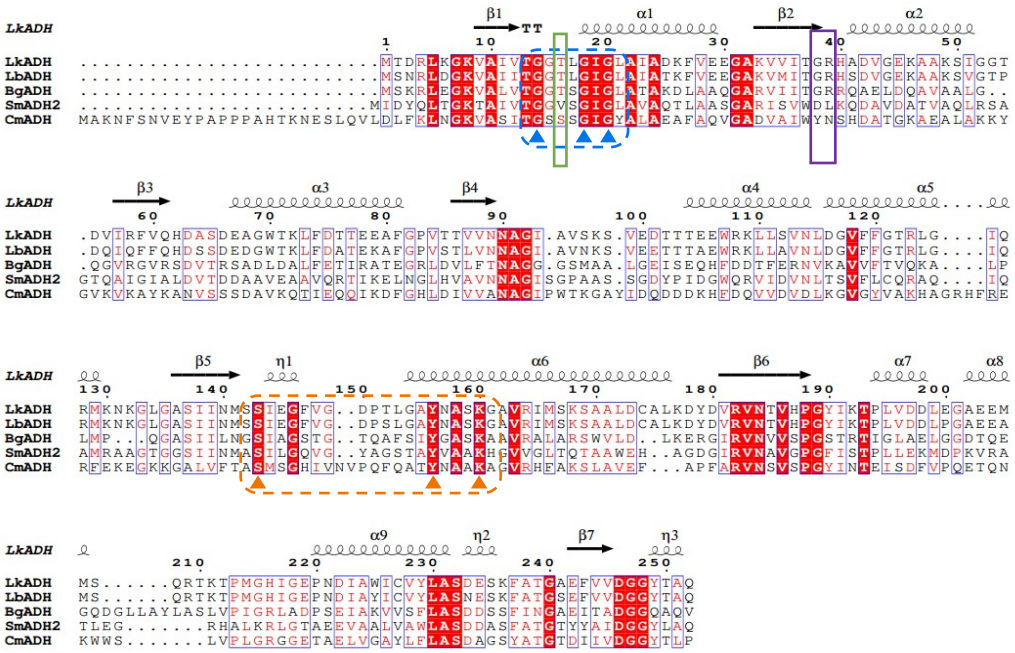

Figure S1. Sequence alignment of *Sm*ADH2, LkADH, LbADH, BgADH and CmADH. Blue triangles represent their conserved residues of the coenzyme binding sites. Orange triangles represent catalytic triads. Green squares and purple squares represent key domains that affect coenzyme dependence.

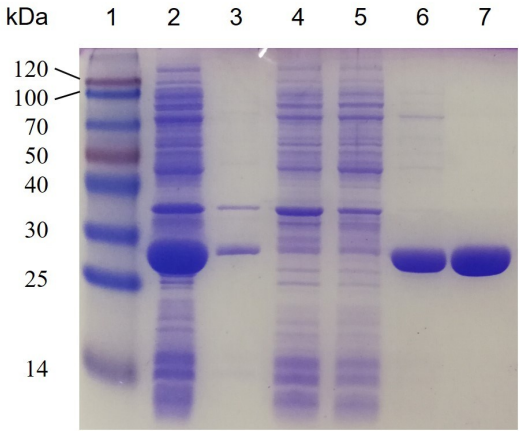

Figure S2. SDS-PAGE analysis of the purified *Sm*ADH2. Lane 1, protein markers. Lane 2, crude enzyme extract. Lane 3, insoluble proteins of cracked *E.coli* BL21(DE3). Lanes from 4 to 6 show collected fractions unabsorbed proteins, diluted by 50 mM PBI and diluted by 100 mM PBI. Lane 7, purified *Sm*ADH2.

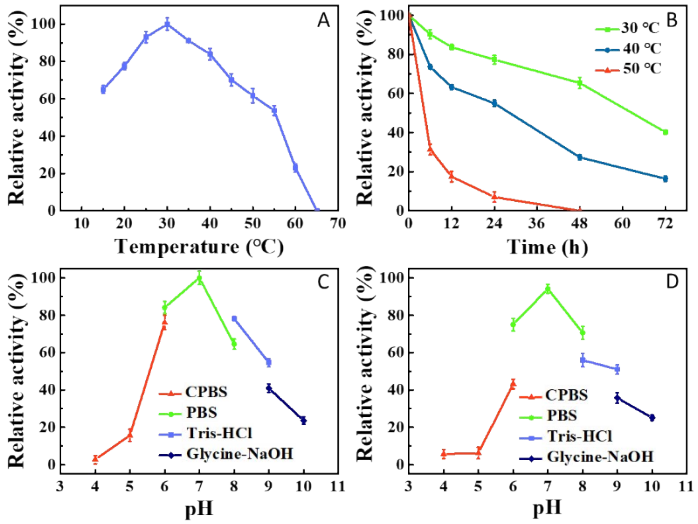

Figure S3. Effects of pH and temperature on specific activity. Each relative activity is shown as a percentage. (A) Optimum temperature of *Sm*ADH2 was studied in the range of 15 °C to 65 °C; (B) Thermal stability was investigated by incubating the purified *Sm*ADH2 at 30 °C 40 °C and 50 °C for 72 h; (C) Optimum pH was tested in 50 mM of the following buffers: sodium citrate (CPBS, pH 4.0-6.0), phosphate buffer saline (PBS, pH 6.0-8.0), Tris-HCl (pH 8.0-9.0) and glycine-NaOH (pH 9.0-10.0); (D) pH stability of *Sm*ADH2 was determined by incubating the enzyme in buffers above at pH values between 4.0-10.0 at 4 °C for 24 h.

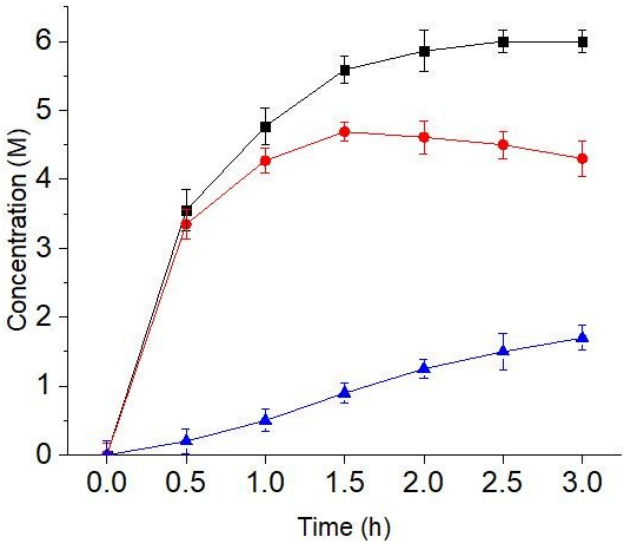

Figure S4. Time-concentration curve of acetone content in each unit in TBCR system. The blue line presents the acetone content in the collection unit. The red line presents the acetone content in the reaction unit. The black line represents the total amount of acetone in the TBCR system. Reaction conditions: 10 ml PBS (100 mM, pH 7.0), 200 mg lyophilized cells, 0 μmol NAD^+, 7.8 g EAA and 5.7 ml 2-propanol (1.25 equiv.) were placed in TBCR (gas flow: 2.5 L min^{-1}; 2-propanol/water ratio: 50%) and reacted at 30 °C for 3 h.

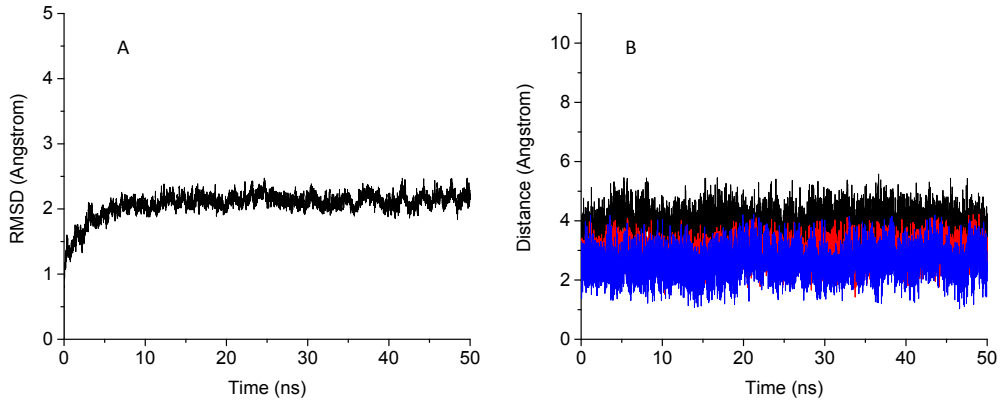

Figure S5. (A) RMSD analysis result. (B) The distances between the carbonyl group of EAA and Tyr159, Ser146 and the hydrogen on the C4 of NADH are shown as blue, red and black lines.

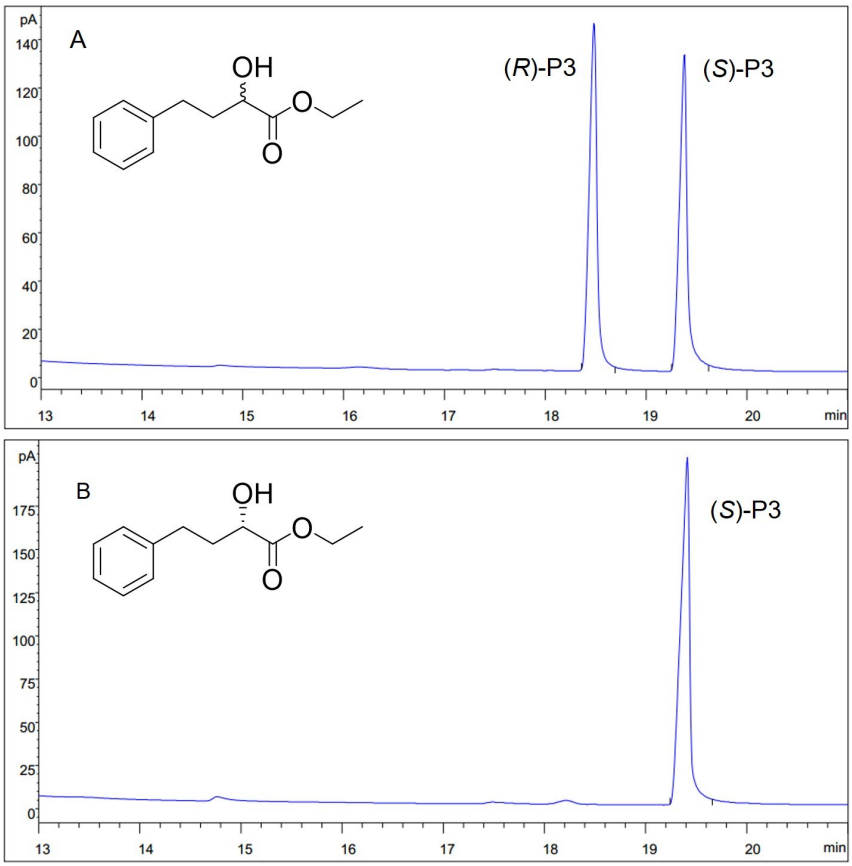

Figure S6. (A) GC analysis of (*S*)-**P3** and (*R*)-**P3**. (B) GC analysis of product **P3** produced by *Sm*ADH2.

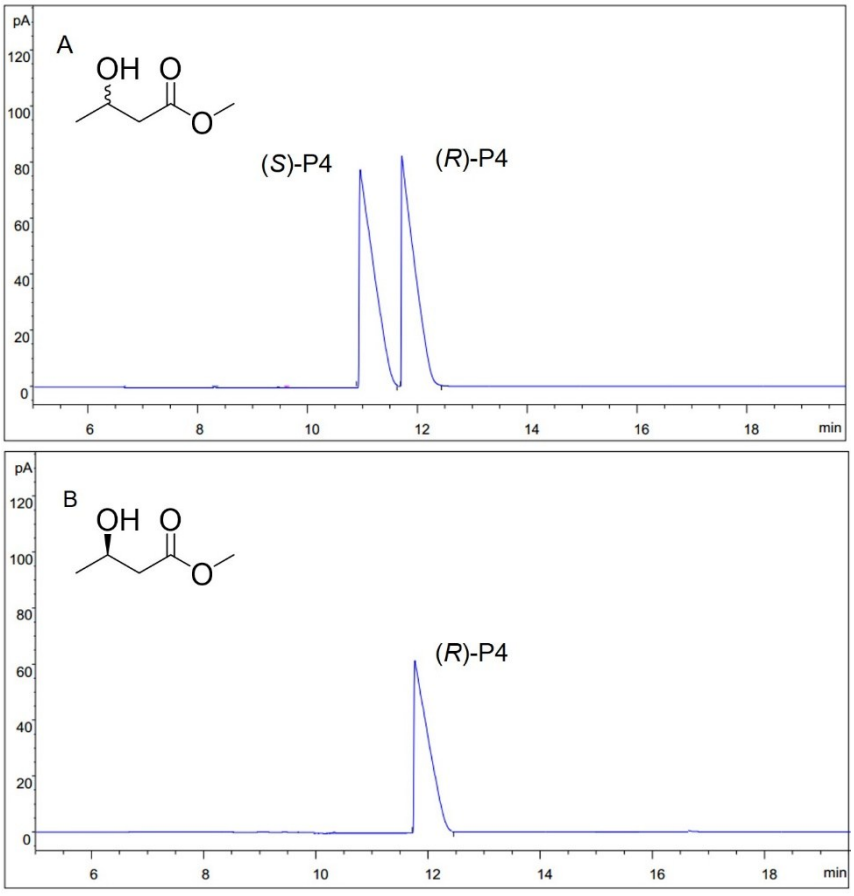

Figure S7. (A) GC analysis of (*S*)-**P4** and (*R*)-**P4**. (B) GC analysis of product **P4** produced by *Sm*ADH2.

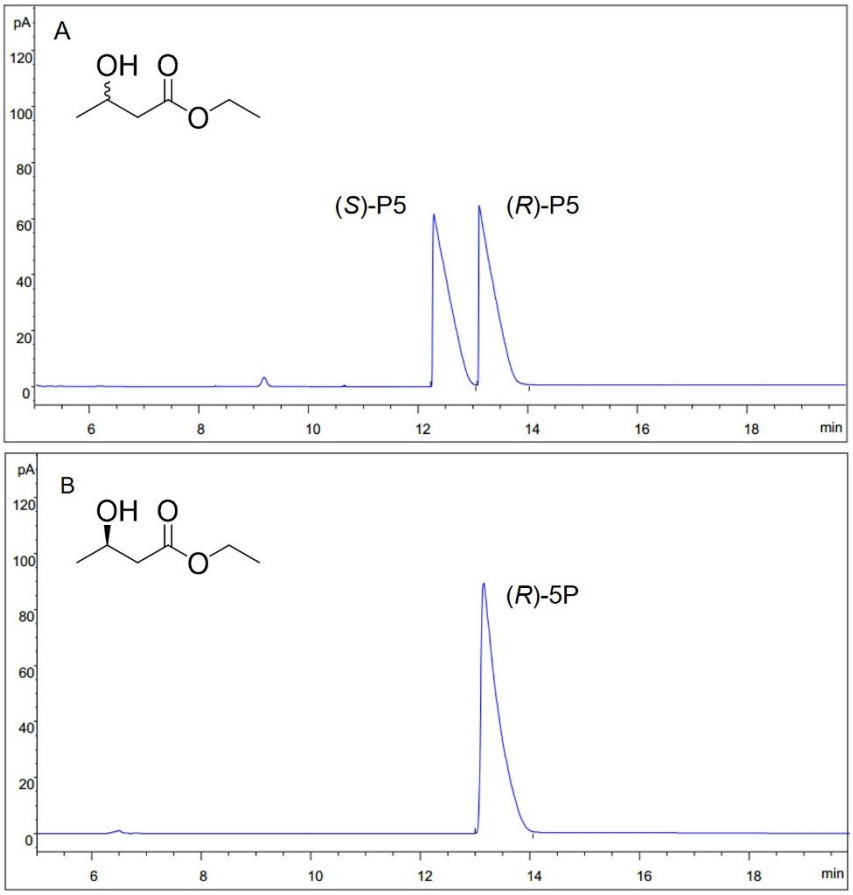

Figure S8. (A) GC analysis of (*S*)-**P5** and (*R*)-**P5**. (B) GC analysis of product **P5** produced by *Sm*ADH2.

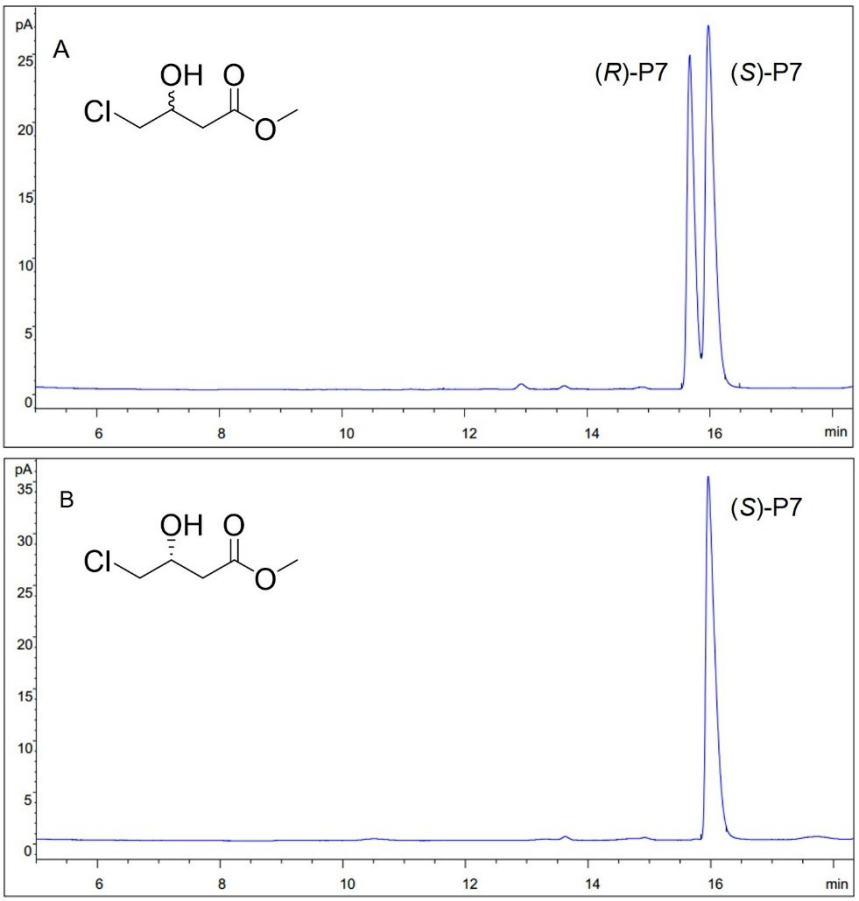

Figure S9. (A) GC analysis of (*S*)-**P7** and (*R*)-**P7**. (B) GC analysis of product **P7** produced by *Sm*ADH2.

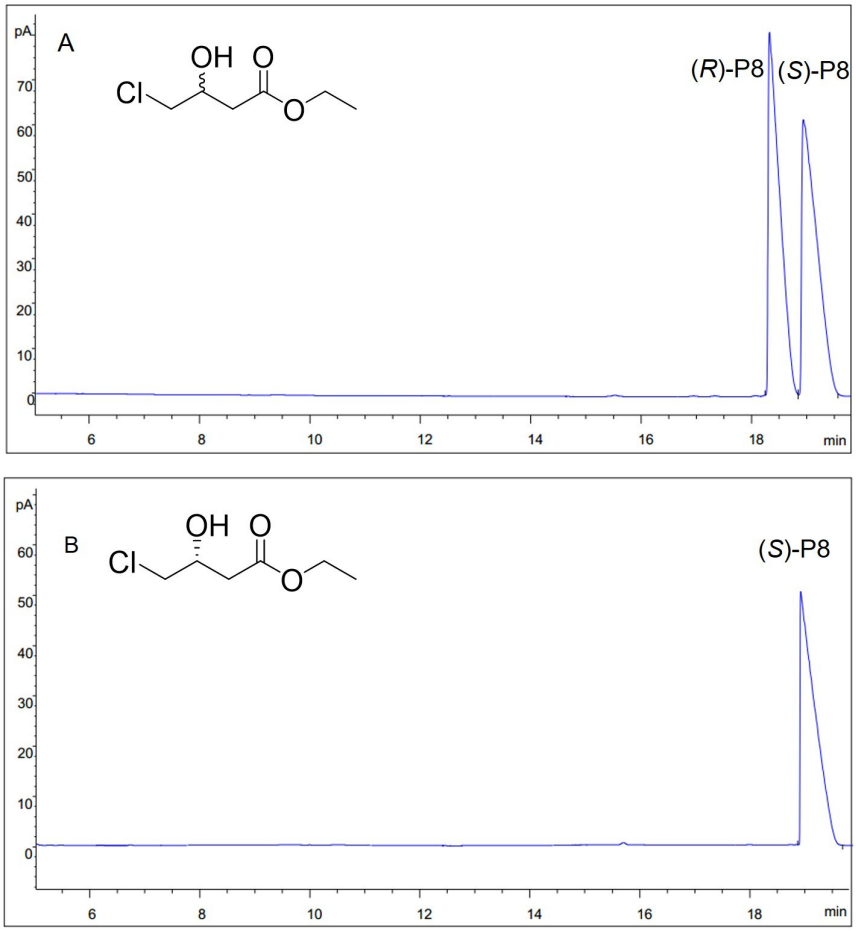

Figure S10. (A) GC analysis of (*S*)-**P8** and (*R*)-**P8**. (B) GC analysis of product **P8** produced by *Sm*ADH2.

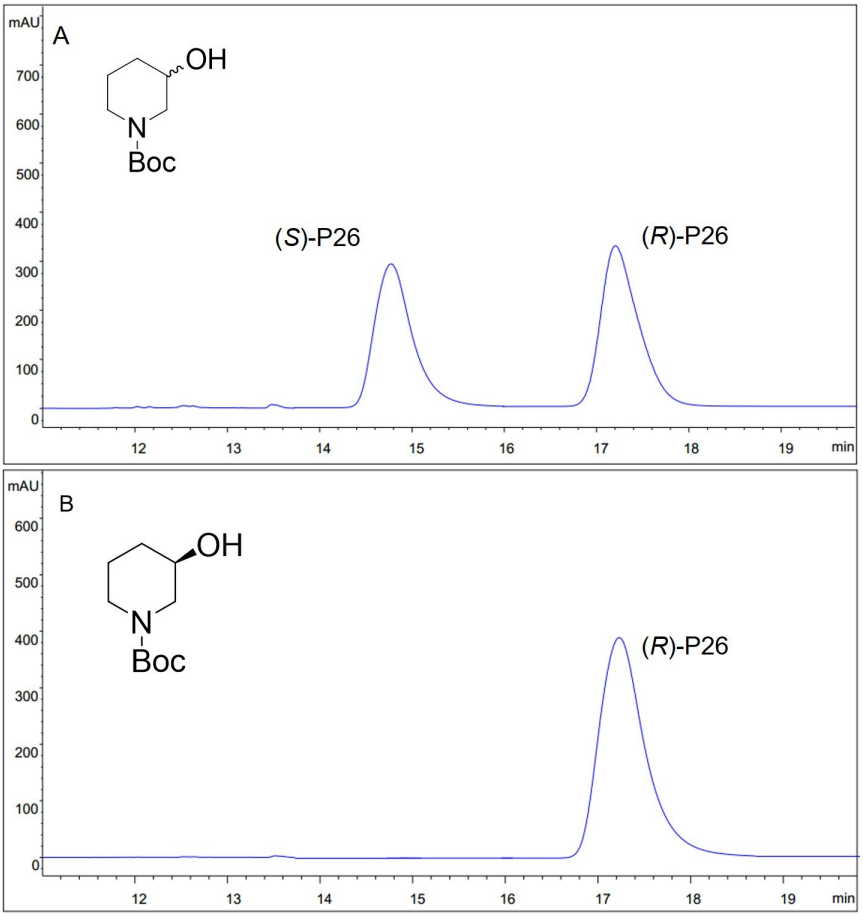

Figure S11. (A) GC analysis of (*S*)-**P26** and (*R*)-**P26**. (B) GC analysis of product **P26** produced by *Sm*ADH2.

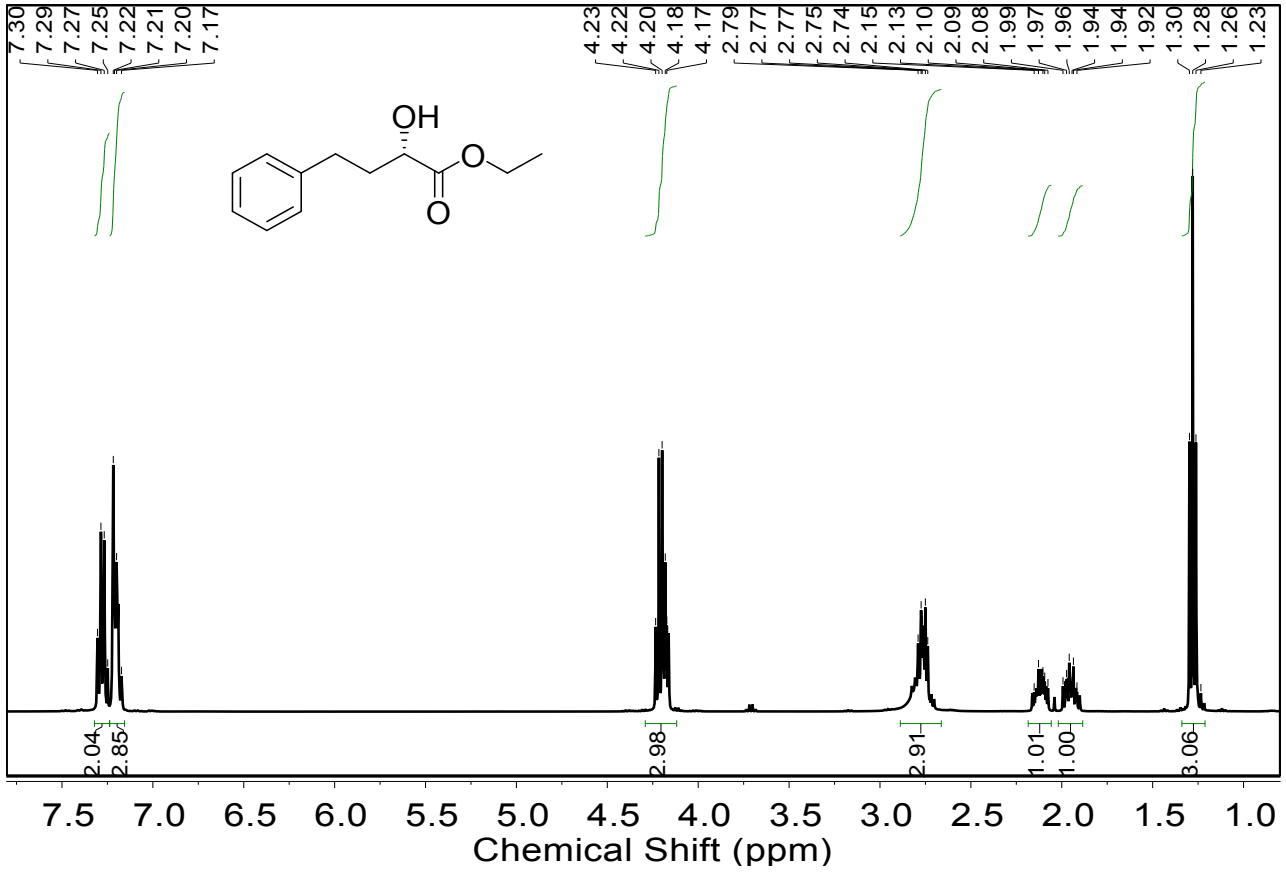

Figure S12. ^{1}H NMR spectrum of (*S*)-**P3**. ^{1}H NMR (400 MHz, Chloroform-*d*) δ 7.28 (q, *J* = 7.6 Hz, 2H), 7.24 – 7.16 (m, 3H), 4.29 – 4.12 (m, 3H), 2.89 – 2.66 (m, 3H), 2.18 – 2.06 (m, 1H), 2.02 – 1.88 (m, 1H), 1.28 (t, *J* = 7.1 Hz, 3H).

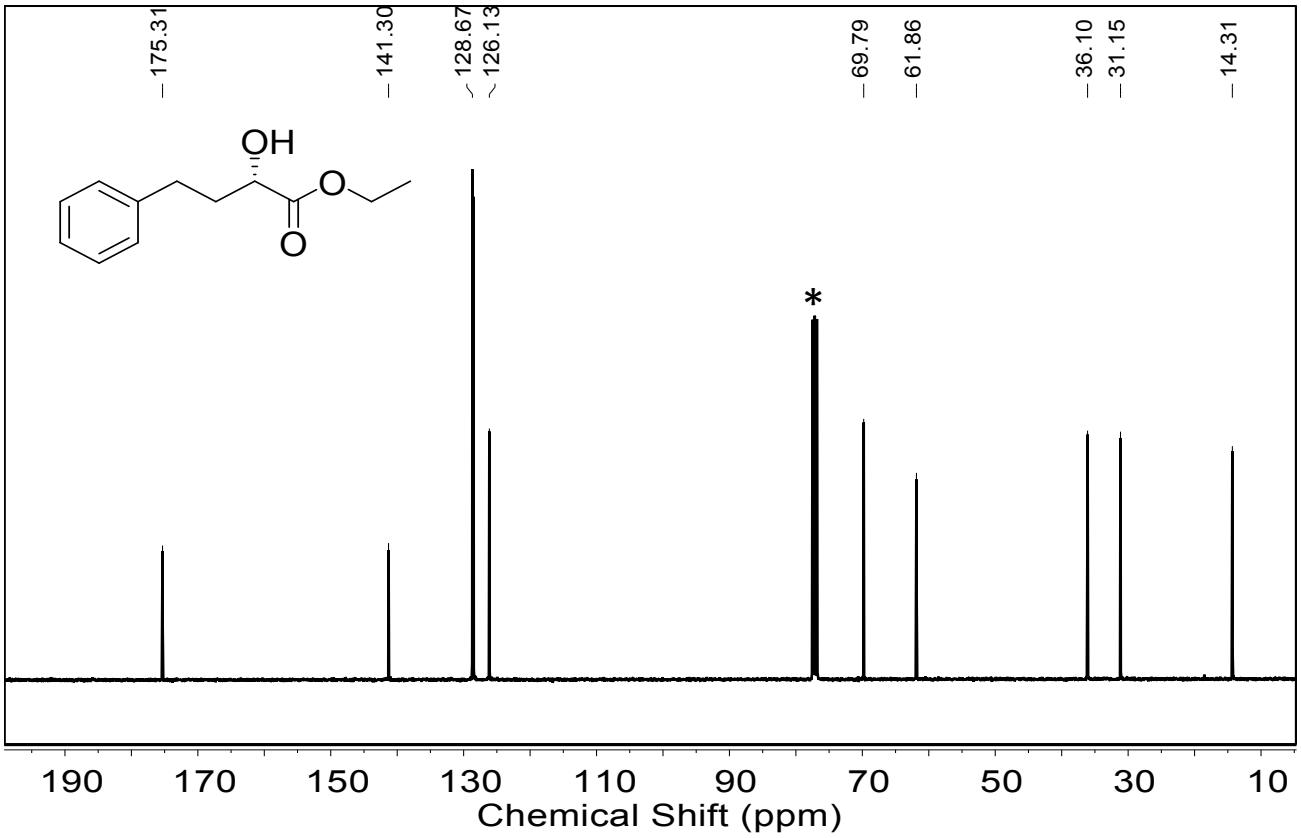

Figure S13. ^{13}C NMR spectrum of (*S*)-**P3**. ^{13}C NMR (101 MHz, Chloroform-*d*) δ 175.31 , 141.30 , 128.67 , 126.13 , 69.79 , 61.86 , 36.10 , 31.15 , 14.31 .

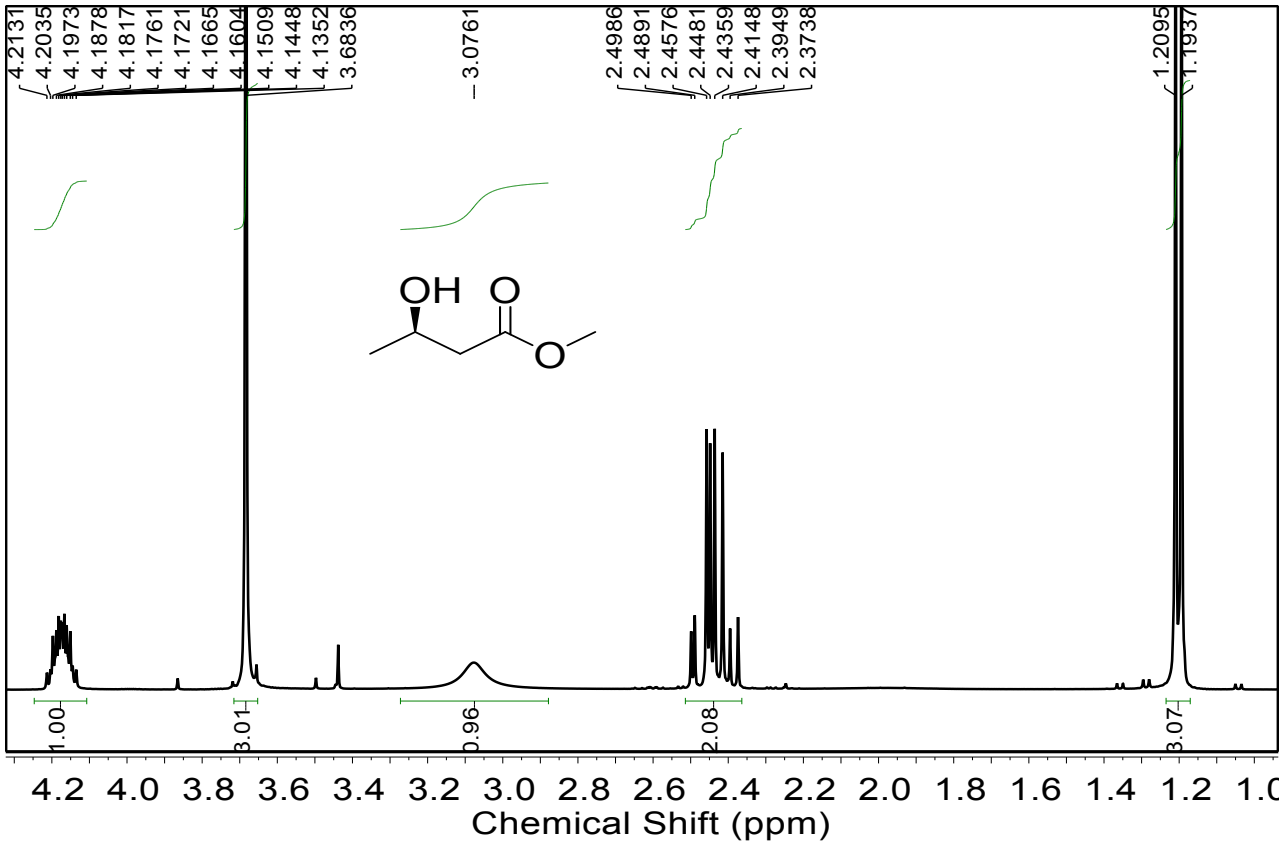

Figure S14. ^{1}H NMR spectrum of (*R*)-**P4**. ^{1}H NMR (400 MHz, Chloroform-*d*) δ 4.17 (dtt, *J* = 12.6, 6.3, 3.2 Hz, 1H), 3.68 (s, 3H), 3.08 (s, 1H), 2.51 – 2.36 (m, 2H), 1.20 (d, *J* = 6.3 Hz, 3H).

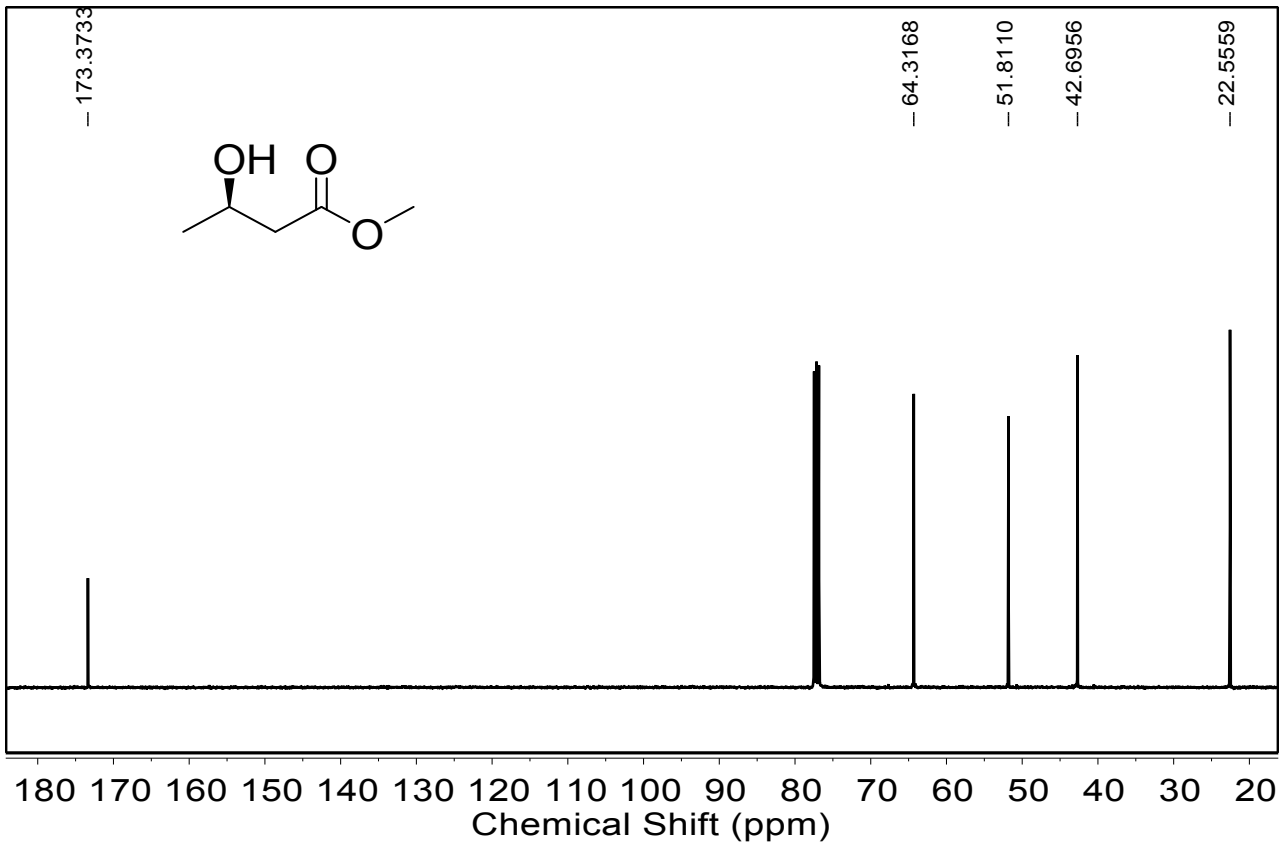

Figure S15. ^{13}C NMR spectrum of (*R*)-**P4**. ^{13}C NMR (101 MHz, Chloroform-*d*) δ 173.37 , 64.32 , 51.81 , 42.70 , 22.56 .

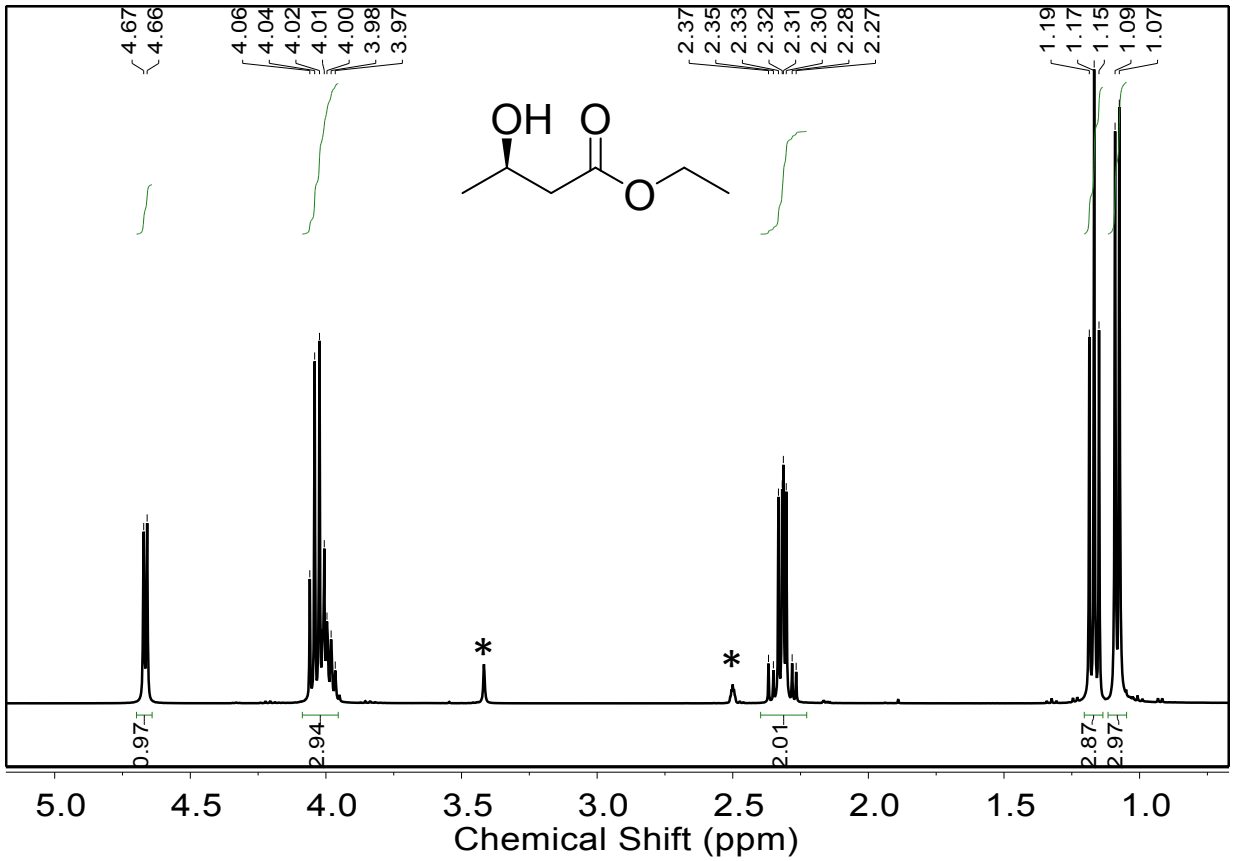

Figure S16. ^{1}H NMR spectrum of (*R*)-**P5**. ^{1}H NMR (400 MHz, DMSO-d_6) δ 4.67 (d, J = 5.1 Hz, 1H), 4.09 – 3.95 (m, 3H), 2.40 – 2.23 (m, 2H), 1.17 (t, J = 7.1 Hz, 3H), 1.08 (d, J = 6.3 Hz, 3H). * H_2O (3.42ppm) and $(CD_3)_2SO$ (2.5ppm)

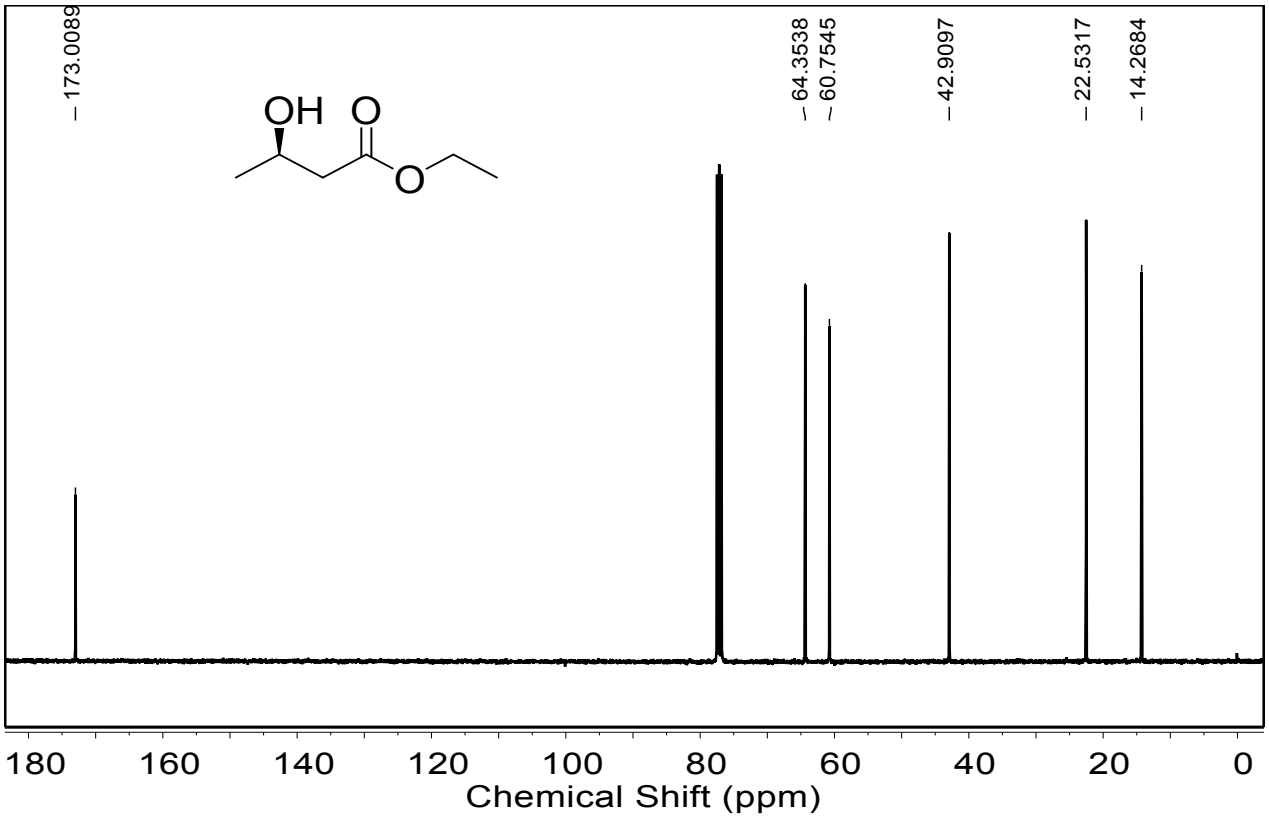

Figure S17. ^{13}C NMR spectrum of (*R*)-**P5**. ^{13}C NMR (101 MHz, Chloroform-*d*) δ 173.01 , 64.35 , 60.75 , 42.91 , 22.53 , 14.27 .

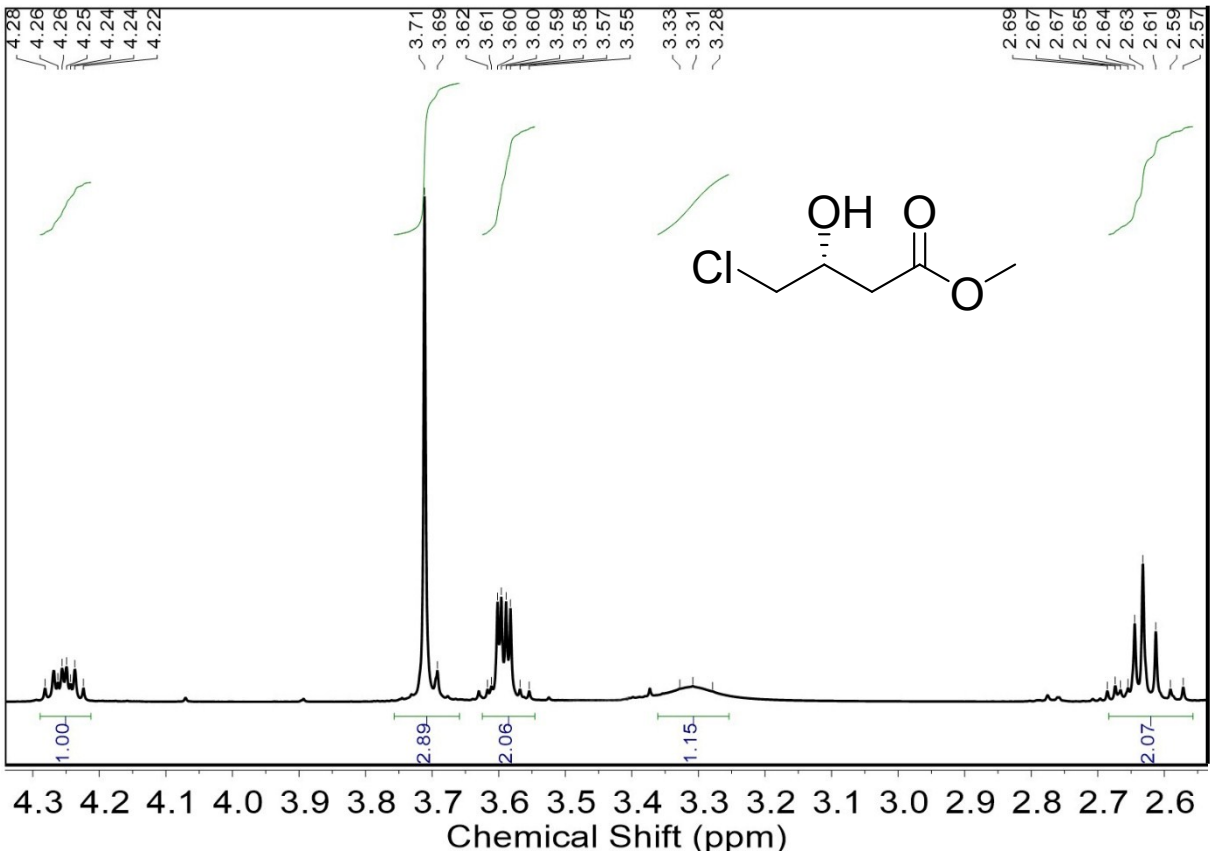

Figure S18. ^{1}H NMR spectrum of (*S*)-**P7**. ^{1}H NMR (400 MHz, Chloroform-*d*) δ 4.29 – 4.21 (m, 1H), 3.71 (s, 3H), 3.60 (td, J = 5.8, 2.5 Hz, 2H), 3.36 – 3.25 (m, 1H), 2.68 – 2.56 (m, 2H).

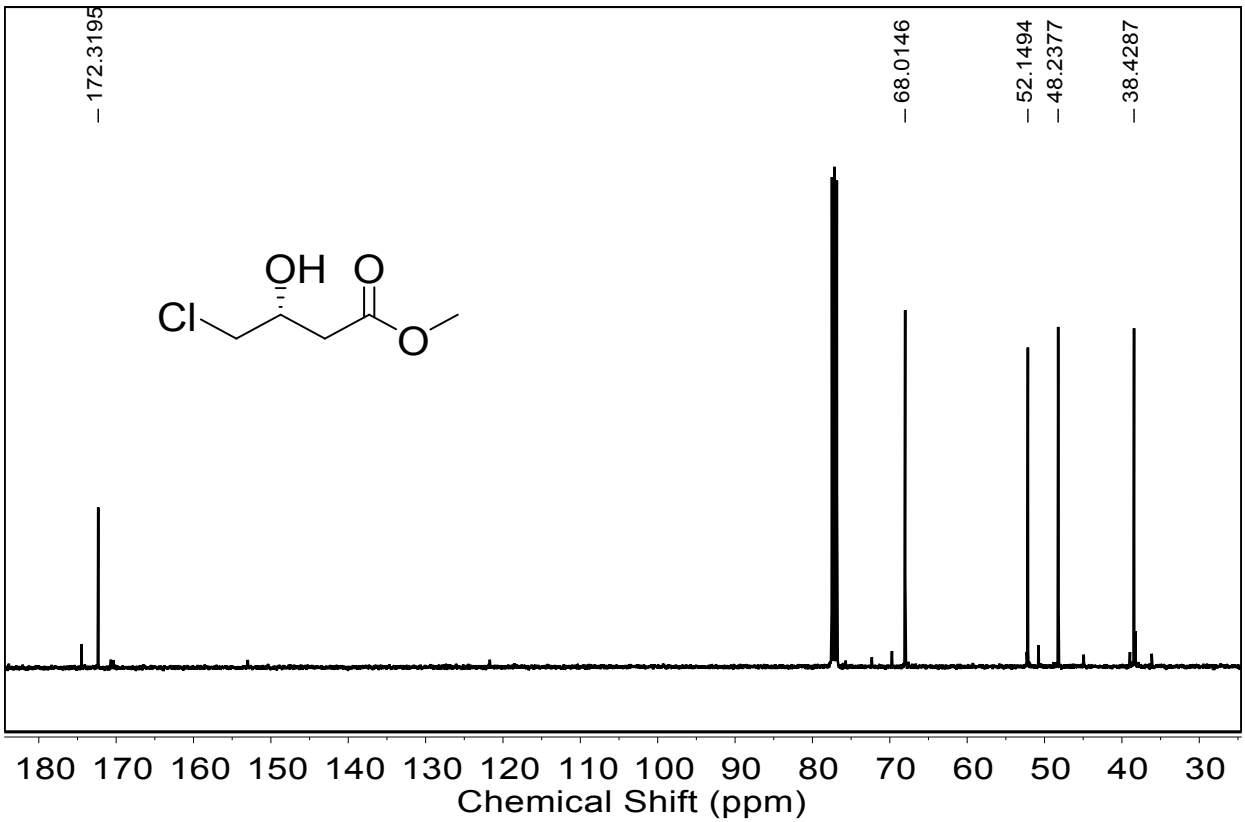

Figure S19. ^{13}C NMR spectrum of (*S*)-**P7**. ^{13}C NMR (101 MHz, Chloroform-*d*) δ 172.32 , 68.01 , 52.15 , 48.24 , 38.43 .

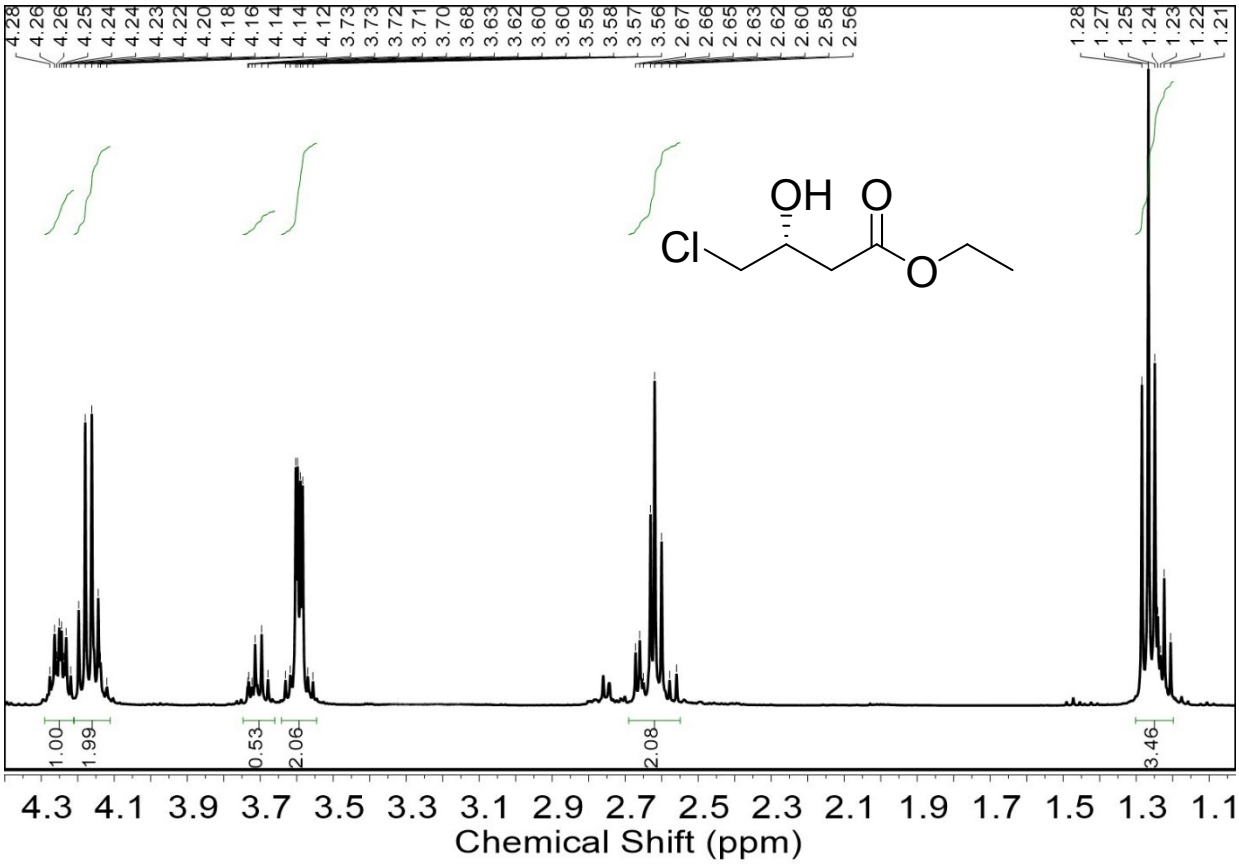

Figure S20. ^{1}H NMR spectrum of (*S*)-**P8**. ^{1}H NMR (400 MHz, Chloroform-*d*) δ 4.25 (dq, J = 7.6, 5.2 Hz, 1H), 4.17 (q, J = 7.1 Hz, 2H), 3.75 – 3.66 (m, 1H), 3.64 – 3.55 (m, 2H), 2.69 – 2.55 (m, 2H), 1.25 (dt, J = 17.2, 7.1 Hz, 3H).

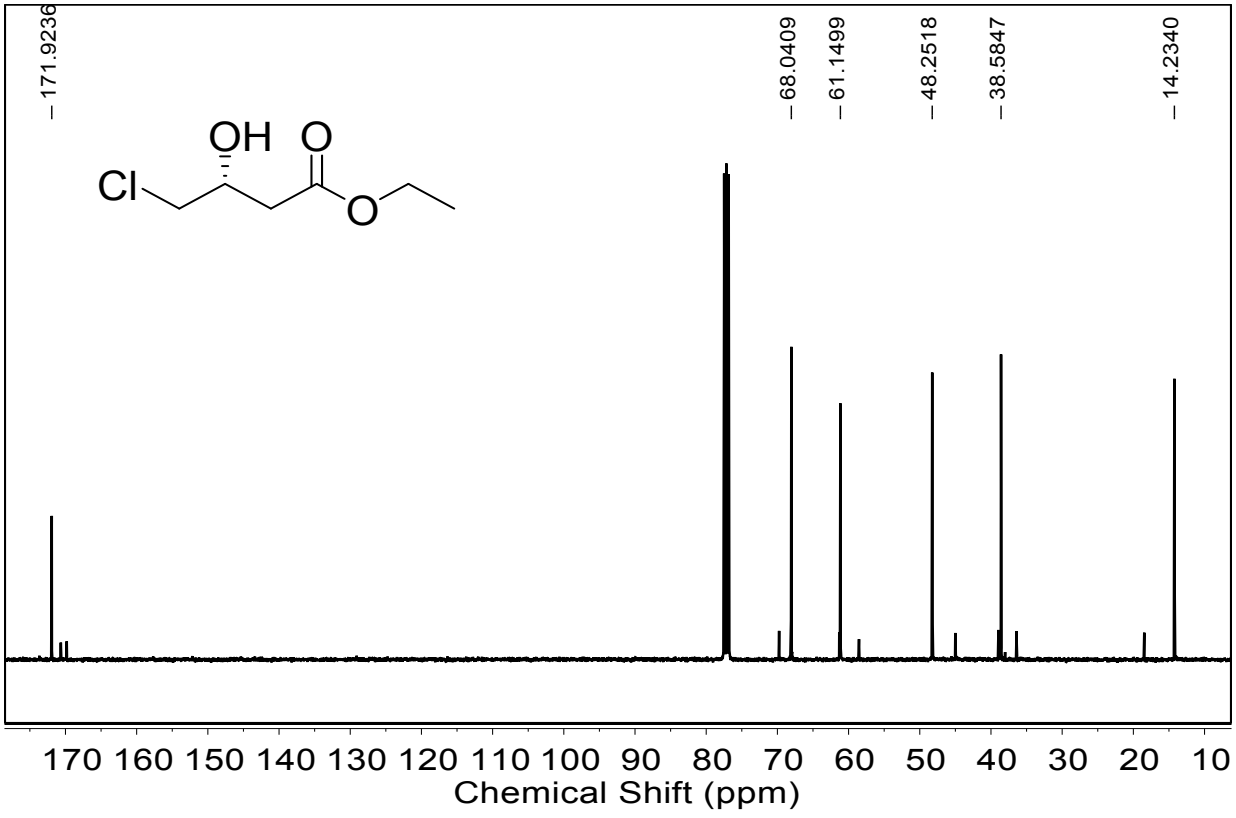

Figure S21. ^{13}C NMR spectrum of (*S*)-**P8**. ^{13}C NMR (101 MHz, Chloroform-*d*) δ 171.92 , 68.04 , 61.15 , 48.25 , 38.58 , 14.23 .

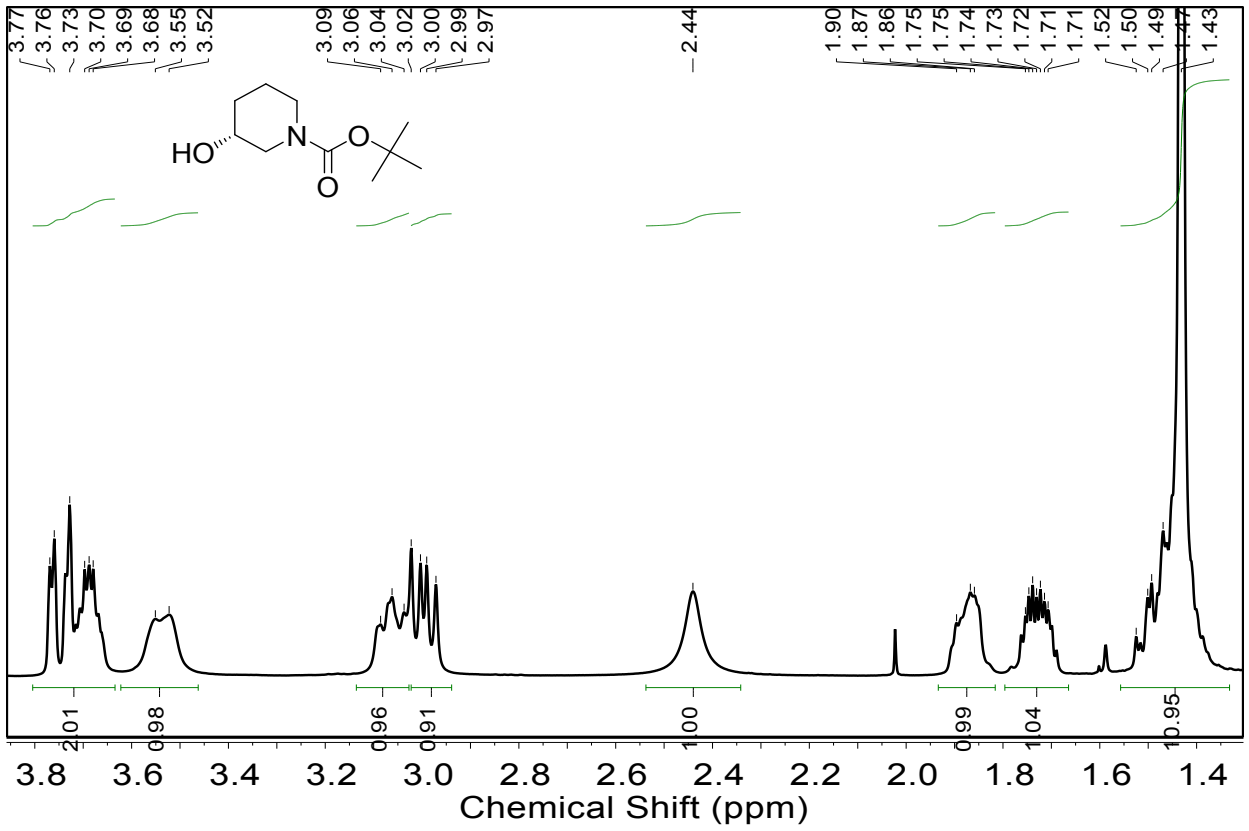

Figure S22. ^{1}H NMR spectrum of (*R*)-**P26**. ^{1}H NMR (400 MHz, Chloroform-*d*) δ 3.80 – 3.63 (m, 2H), 3.54 (d, *J* = 11.4 Hz, 1H), 3.14 – 3.03 (m, 1H), 3.00 (dd, *J* = 12.8, 7.7 Hz, 1H), 2.44 (s, 1H), 1.93 – 1.82 (m, 1H), 1.73 (dq, *J* = 9.5, 2.9 Hz, 1H), 1.43 (s, 11H).

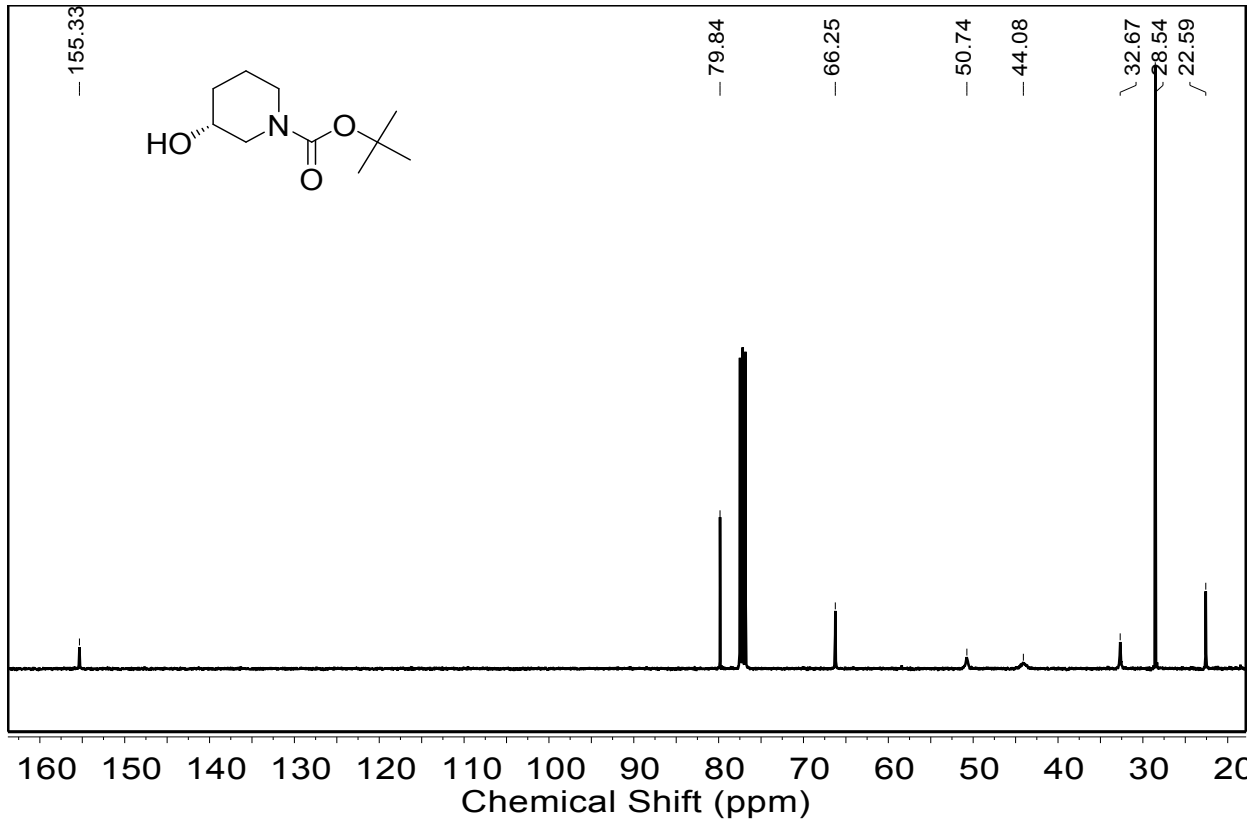

Figure S23. ^{13}C NMR spectrum of (*R*)-**P26**. ^{13}C NMR (101 MHz, Chloroform-*d*) δ 155.33 , 79.84 , 66.25 ,50.74 , 44.08 , 32.67 , 28.54 , 22.59 .